Acta Cryst. (1991). B47, 240–253

Determination and Restrained Least-Squares Refinement of the Structures of Ribonuclease Sa and its Complex with 3′-Guanylic Acid at 1·8 Å Resolution

BY J. SEVCIK

Institute of Molecular Biology, Slovak Academy of Sciences, Dúbravská cesta, 84251 Bratislava, Czechoslovakia

AND E. J. DODSON AND G. G. DODSON*

Chemistry Department, University of York, Heslington, York, YO1 5DD, England

(*Received* 5 *March* 1990; *accepted* 23 *August* 1990)

Abstract

The crystal structures of ribonuclease from *Streptomyces aureofaciens* (RNase Sa) and its complex with 3′-guanylic acid (guanosine 3′-monophosphate, 3′-GMP) have been determined by the method of isomorphous replacement. The atomic parameters have been refined by restrained least-squares minimization using data in the resolution range 10·0–1·8 Å. All protein atoms and more than 230 water atoms in the two crystal structures have been refined to crystallographic *R* factors of 0·172 and 0·175 respectively. The estimated r.m.s. error in the atomic positions ranges from 0·2 Å for well-defined atoms to about 0·5 Å for more poorly defined atoms. There are two enzyme molecules in the asymmetric unit, built independently, and referred to as molecules *A* and *B*. The value of the average *B* factor for protein atoms in both structures is about 19 Å^2 and for water molecules about 35 Å^2. Electron density for the substrate analogue 3′-GMP was found only at the active site of molecule *A*. The density was very clear and the positions of all 3′-GMP atoms were refined with precision comparable to that of the protein.

Introduction

The ribonuclease (E.C.3.1.4.8) from *Streptomyces aureofaciens*, RNase Sa, is a guanylate endoribonuclease, which belongs to the homologous family of microbial ribonucleases (Hill *et al.*, 1983). Typically of this family, the enzyme specifically hydrolyses the phosphodiester bonds of RNA at the 3′-side of guanosine nucleotides (Zelinkova, Bacova & Zelinka, 1971). The enzyme's primary structure, of 96 amino-acid residues, has been determined (Shlyapnikov, Both, Kulikov, Dementiev, Sevcik & Zelinka, 1986). The relative molecular weight is 10 544. The amino-acid sequence of RNase Sa is shown in Fig. 1. In contrast to the other microbial ribonucleases, there is one insertion into the RNase Sa sequence, Thr 76. The microbial RNases are believed to catalyse the specific cleavage of RNA with the same chemical mechanism as RNase A (Findlay, Herries, Mathias, Ranbin & Ross, 1961; Takahashi, 1970; Takahashi & Moore, 1982). The active-site residues of RNase Sa have been studied by various techniques: chemical modifications, NMR spectroscopy, kinetic measurements, circular dichroism. Some of the active-site residues have been identified (Both, Zachar & Zelinka, 1984). The crystal structures of the enzyme and that of its complex with 3′-GMP have been determined; these confirm the identities of the catalytic residues and provide experimental support for the proposed mechanism of its catalytic action.

Experimental

The enzyme RNase Sa was isolated from a culture medium of *S. aureofaciens* (Bacova, Zelinkova & Zelinka, 1971) and highly purified (Gasperik, Prescakova & Zelinka, 1982). The crystals were grown from solutions of phosphate buffer at pH 7·2

```
D-V-S-G-T-V-C-L-S-A-L-P-P-E-A-T-D-T-L-N-L-I-A-S-D-G-P-F-P-Y-
                  10                  20                  30

     +    +  * + *    + +              *
S-Q-D-G-V-V-F-Q-N-R-E-S-V-L-P-T-Q-S-Y-G-Y-Y-H-E-Y-T-V-I-T-P-
                  40                  50                  60

       +      *                       +  + * +     +
G-A-R-T-R-G-T-R-R-I-I-C-G-E-A-T-Q-E-D-Y-Y-T-G-D-H-Y-A-T-F-S-
                  70                  80                  90

L-I-D-Q-T-C
```

Fig. 1. The primary structure of RNase Sa. The residues which are conserved in most of the known microbial RNases are marked by * (Asn 39, Glu 41, Glu 54, Arg 69, His 85). In addition, in prokaryotic ribonucleases, a subgroup to which RNase Sa belongs, conserved residues are marked by + (Gly 34, Phe 37, Arg 40, Leu 44, Pro 45, Arg 65, Thr 82, Asp 84, Tyr 86, Phe 89).

* To whom correspondence should be addressed.

0108-7681/91/020240-14$03.00

Table 1. *Data collection and processing statistics*

	Native	Mercury	Platinum	Iodine	Platinum	Native	3′-GMP
Resolution (Å)	2·5	3·15	6·0	2·5	2·5	1·8	1·8
Method	Diffractometer	Diffractometer	Diffractometer	Rotation camera	Rotation camera	Rotation camera	Rotation camera
Wavelength (Å)	1·542	1·542	1·542	1·542	1·542	1·488	1·488
Rotation axis	*c*	*c*	*c*	*c*/*b*	*c*/*b*	*c*/*a*	*c*/*b*
Unit-cell dimensions (Å)							
a	64·90	64·90	64·97	65·00	64·85	64·88	64·79
b	78·32	78·32	78·75	78·66	78·56	78·69	78·13
c	38·79	38·79	39·55	38·81	39·51	39·17	38·85
Total No. of measurements	9626	12642	3558	26846	29631	85946	85834
No. of independent reflections	7122	3640	499	6871	6839	17202	17105
No. of anomalous measurements		3325	306	5616	5671		
Merging *R*	0·055	0·124	0·057	0·075	0·057	0·056	0·117

by the vapour-equilibration technique using ammonium sulfate as precipitant (Sevcik, Gasperik & Zelinka, 1982). The crystal space group is $P2_12_12_1$ with cell dimensions: $a = 64{\cdot}90$ (2), $b = 78{\cdot}32$ (2), $c = 38{\cdot}79$ (2) Å. The crystals have a regular morphology and grow in size up to $1{\cdot}4 \times 0{\cdot}8 \times 0{\cdot}4$ mm. They diffract very strongly and, with synchrotron radiation, data extend to beyond 1·3 Å spacing.

An attempt to solve the structure by molecular-replacement calculations failed. The self-rotation function contained no obvious peaks from which symmetry relations between the molecules could be deduced. No accurate coordinates of a homologous ribonuclease were available at this stage which made the isomorphous heavy-atom approach to phasing the only alternative.

Three heavy-atom derivatives were prepared by diffusion of heavy-atom compounds into crystals. The heavy-atom derivative crystals contain mercury (mersalyl), platinum (potassium tetranitro platinum) and iodine. Solid mersalyl and potassium tetranitro platinum, respectively, were added to drops containing crystals until the solution was saturated. The reagents were left in the mother liquor surrounding the RNase Sa crystals for a week. The iodine derivative was prepared by adding a saturated aqueous solution of I_2/KI and $C_2H_2O_4$ to drops containing crystals until they turned permanently yellow–brown. The iodination reaction with the enzyme in the crystals was complete in about 1 h. A similar diffusion method was used to prepare the RNase Sa–3′-GMP complex crystals.

The X-ray diffraction data were collected using a Hilger–Watts diffractometer and an Arndt–Wonacott rotation camera. Three sets of data, including Friedel equivalents, were collected with the diffractometer working in the ω-scan mode; stationary background measurements were made on both sides of each reflection. The data sets were placed on a common scale after the usual semi-empirical corrections for absorption (North, Phillips & Mathews, 1968).

Data sets of the native crystal, iodine and platinum derivatives and the 3′-GMP complex were collected by film methods. For the iodine and platinum derivative crystals, data were collected to 2·5 Å resolution using a Cu $K\alpha$ conventional sealed beam tube (wavelength 1·5418 Å, $U = 40$ kV, $I = 20$ mA). The rotation angle was 2° per photograph. Intensities in the principal set of data were recorded in an angular range 0–96°. Blind-region data were collected from the same crystal in an angular range 0–22° after remounting the capillary on the goniometer head.

High-resolution data (to 1·8 Å resolution) were collected from crystals of native RNase and its complex with 3′-GMP at the Synchrotron Radiation Source at Daresbury. The wavelength of radiation used was 1·488 Å. The rotation angle per photograph was 1·5°. Intensities in the principal set were recorded in an angular range 0–96° and in the blind region in the range 0–36° from the same crystal. The intensities from the films were measured by an on-line Joyce–Loebel Scandig 3 densitometer in 2 OD range with 100 μm sampling intervals for 2·5 Å data and 50 μm sampling intervals for 1·8 Å data. Digitized intensities were processed by the *Programme Suite for Protein Crystallography*, Daresbury Laboratory, England. Absorption corrections were not applied. The data sets collected by diffractometer were used to complete the photographic data sets with reflections which were either unusable owing to saturation or absent owing to geometrical cut-off.

Details of the collected data sets are given in Table 1, where crystals are named according to their substitution; native refers to the free enzyme. The table gives the resolution limit to which the data were collected, the method of data collection, the wavelength of radiation used, the rotation axis for collecting data in the principal/blind region, the unit-cell parameters as obtained from diffractometer measurements and refinement of each film data set, the total number of measurements, the number of independent reflections, the number of anomalous measurements for heavy-atom derivative crystals, and the merging R factor defined by $R_{\text{merge}} = \sum[I(i) - \langle I\rangle]/\sum I(i)$, where $I(i)$ are intensity values for individual measurements and $\langle I\rangle$ those of corresponding mean values. The summation is over all measurements.

By the criterion of their internal agreement, the data sets proved to be of good quality but there was a problem with the data sets from the 3′-GMP–enzyme complex crystal. Here the blind-region data agreed poorly with the principal-axis data. The R_{merge} value for the principal data set was 0·052 and for the blind region 0·063. After merging these two sets of data the R_{merge} value was 0·117. This discrepancy is not easily explained. It is associated with a change in the operation mode of the Synchrotron Radiation Source to the 'single-bunch mode' prior to collecting the blind-region data. More probably, however, the poor agreement is caused by absorption effects. For this set of data a procedure, known as a postrefinement was used (Evans, 1987; Winkler Schutt & Harrison, 1979).

Determination of the crystal structure

The positions of the five platinum and two mercury sites were determined by direct methods with *MULTAN* (Wilson, 1978). They were also identified from the difference Patterson function with coefficients $|F_{PH} - F_P|$, where F_P are the observed amplitudes of the protein and F_{PH} are those for the heavy-atom derivatives. All of the platinum sites were identified clearly as peaks in the Patterson maps. Analysis of the iodine derivative Patterson and *MULTAN* maps, however, led to inconsistent peaks. The positions of six I atoms were determined from difference Fourier calculations using phases derived from the platinum derivative data. Not all of these were consistent with the Patterson and *MULTAN* solutions; this discrepancy was recognized as indicating that the iodine derivative might not yield good phases.

The coordinates of the heavy atoms were refined by least-squares minimizations to the experimental heavy-atom contribution F_{HLE} (Dodson, 1975). The heavy-atom statistics are given in Table 2, while the coordinates of heavy atoms determined from the Patterson maps and those determined from the refined structure are given in Table 3.

Comparison of atom coordinates determined from Patterson and *MULTAN* synthesis and those from the refined structure confirms the isomorphism of platinum substitution. Analysis of the platinum-reacted enzyme revealed that there are two binding sites for molecule *A* and three for molecule *B*. Binding of the Pt atom to His 53*A* is shown in Fig. 2. In molecule *B* the His 85 imidazole ring has two distinct positions of its side chain to which Pt3 and Pt5, respectively, are bound (Fig. 3). These two positions imply rotation of the imidazole ring around the Cα—Cβ bond. Disorder of the His 85*B* residue was not observed in either the native enzyme or its complex with 3′-GMP which bonds to the His 85 side chain.

Table 2. *Heavy-atom statistics*

$R_D = \sum|F_P - F_{PH}|/\sum F_P$, Cullis factor $R_C = \sum_i|F_{PHcalc} - F_{PHobs}|/\sum F_{PHobs}$ (for centric terms only), phasing power = r.m.s. heavy-atom structure factor/r.m.s. lack of closure.

	R_D	R_C	Phasing power Real	Anom.
Platinum	21·62	51	1·8	0·6
Iodine	29·30	65	1·1	0·8
Mercury	17·93		1·0	–

Analysis of the iodine derivative was only partially successful. The Patterson peaks lay near special positions which complicated their analysis. I-atom positions deduced from the Patterson maps did not occur in the *MULTAN* maps. The difference Fourier map calculated with phases determined from the platinum derivative showed six iodine sites; only the major sites were satisfactorily consistent with the *MULTAN* and Patterson peaks. The behaviour suggested there was some loss of isomorphism in the derivative. Six sites were however finally selected and refined and used in the phase calculation.

As noted earlier there were some difficulties in determining the iodine positions. The difference map calculated with the refined phases showed some of the positions used in the phase determination were in error or had insignificant occupancy (sites I3, I4 and I6, see Table 3), and were a result of protein movements at the reaction sites. As a result there was a significant loss of isomorphism caused by iodination even though the axial lengths were not altered by the reaction. The details of the structural changes in these crystals associated with iodination are now being carefully investigated.

Several electron density maps were calculated at different resolutions and plotted on transparent plastic sheets. Their phases were derived from all three derivative data sets with Blow & Crick's (1959) combination procedure applied to both the isomorphous and anomalous differences. The most useful map was that calculated with combined isomorphous phases to 2·5 Å resolution and to which solvent-flattening procedures were then applied (Wang, 1985). These procedures significantly improved the phasing used in the calculation of the electron density map and enabled a well-defined border between solvent and protein to be determined. For comparison one section of the map calculated before and after the solvent-flattening procedures is shown in Figs. 4(*a*) and 4(*b*). The quality of the solvent-flattened map was further improved by collecting a 6 Å diffractometer data set from a platinum derivative crystal which was used to fill in the low-order data missing from the film data. In this map the β-sheet structure and the α helix for both molecules were located first. Finding the mutual orientation of

Table 3. *Heavy-atom parameters*

	Binding site	Refined to F_{HLE} Occupancy	x	y	z	Refined coordinates Occupancy	x	y	z
Hg1	His 85*B*	0·200	0·110	0·900	0·200		0·108	0·902	0·202
Hg2	His 53*A*	0·200	0·158	0·445	0·033		0·157	0·445	0·023
Pt1	His 85*A*	0·416	0·567	0·829	0·018	0·381	0·566	0·827	0·017
Pt2	His 53*A*	0·384	0·842	0·945	0·467	0·345	0·843	0·943	0·467
Pt3	His 85*B*	0·365	0·103	0·940	0·194	0·264	0·105	0·942	0·199
Pt4	His 53*B*	0·332	0·190	0·006	0·744	0·334	0·191	0·006	0·743
Pt5	His 185*B*	0·209	0·045	0·852	0·277	0·190	0·050	0·847	0·247
I1	Asp 84*B*	0·946	0·081	0·773	0·139	0·332	0·081	0·765	0·126
I2	His 85*A*	0·547	0·068	0·739	0·001	0·502	0·082	0·732	0·006
I3	Glu 54*A*	0·170	0·595	0·994	0·034	0·142	0·594	0·899	0·020
I4	His 85*A*	0·286	0·132	0·709	0·065	0·049	0·133	0·722	0·074
I5	Tyr 49*A*	0·238	0·713	0·983	0·090	0·204	0·706	0·965	0·094
I6	Tyr 59*B*	0·450	0·897	0·807	0·101	0·078	0·881	0·788	0·131

these two structural features between molecules *A* and *B* was rather difficult owing to the confusion created by the Hg and I atoms not binding to the same amino-acid residues in both molecules. It is worth noting that the different binding sites for the Hg and I atoms in molecules *A* and *B* can only partly be explained by steric hindrance. This unexpected behaviour was not recognized at this stage. After the orientation of the two independent molecules was established, determination of the backbone for both molecules in the asymmetric unit was straightforward, except for several residues at the chain termini, where the connectivity was not easily disentangled. The highly aromatic sequence, Tyr-Tyr-His-Glu-Tyr-Thr (residues 51–56), was unambiguously identified at this stage. Coordinates for about 50 identifying positions in the backbone of each molecule were recorded and used to label the backbone when displaying the map on the Evans & Sutherland PS300 graphics system. Both molecules in the asymmetric unit were built according to their primary structure using the program *FRODO* (Jones, 1978).

Experiments to extend the phases to higher resolution were carried out using solvent-flattening procedures (Wang, 1985). The phases were calculated in the range 2·5 to 1·8 Å in seven steps increasing the resolution limit by 0·1 Å in each step. The map calculated from these structure factors at 1·8 Å resolution was, however, only in some regions an improvement on that calculated to 2·5 Å spacing, but it was also used in the process of building the model since it gave useful supplementary information.

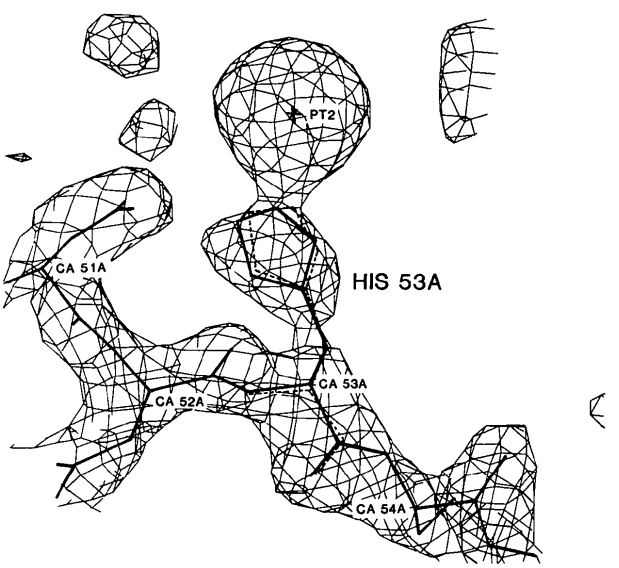

Fig. 2. Binding of the platinum atom to His 53 in molecule *A* in the platinum derivative. The electron density is obtained from the $2F_o$(Pt) − F_c Fourier map and is contoured at approximately 0·7 e Å^{-3}; the same contouring level is used in all other electron density figures. The dotted lines correspond to the atomic positions of the histidine 53 in the native structure [crystal structure (1)].

Structure refinement

The native enzyme: crystal structure (1)

The atomic positions were refined by the stereochemically restrained least-squares method (Hendrickson & Konnert, 1980; Hendrickson, 1985) in about 150 cycles and 13 sessions of model building carried out on an Evans & Sutherland colour graphics system using the program *FRODO* (Jones, 1978). The residual index, R, for the initial and incomplete model was 0·52. In this model about 12 residues in each molecule were excluded.

In the early stages, while the R value was above 0·30, the map calculated from isomorphous phases improved by solvent flattening was used as a reference. Throughout the refinement process Fourier maps with coefficients $(2F_o - F_c)$ and $(3F_o - 2F_c)$ were calculated (Vijayan, 1980); the latter proved to be more useful in the determination of some parts of the structure. In the later stages of refinement difference Fourier maps with coefficients $(F_o - F_c)$ were used, mainly to determine the positions of water molecules and those parts of the structure, mostly side chains, which were more poorly defined.

Such parts were excluded from the electron density calculations at selected stages in order to reduce to a minimum the influence of incorrectly placed atoms on the electron density. After each manual rebuilding of the model the geometrical restraints were loosened to give the atoms more freedom of movement, while in the last refinement cycles the geometry was tightened in order to improve the stereochemistry of the model. In each round, which consisted of about ten refinement cycles, at least two cycles were applied to refine the temperature factors. The refinement finally converged to a crystallographic R value of 0·17. At this stage there were no electron density peaks higher than 0·3 e $Å^{-3}$ in the $F_o - F_c$ map. In the refinement 17 579 reflections were used (in the range 10–1·8 Å). The progress of the refinement calculations is illustrated in Fig. 5(*a*).

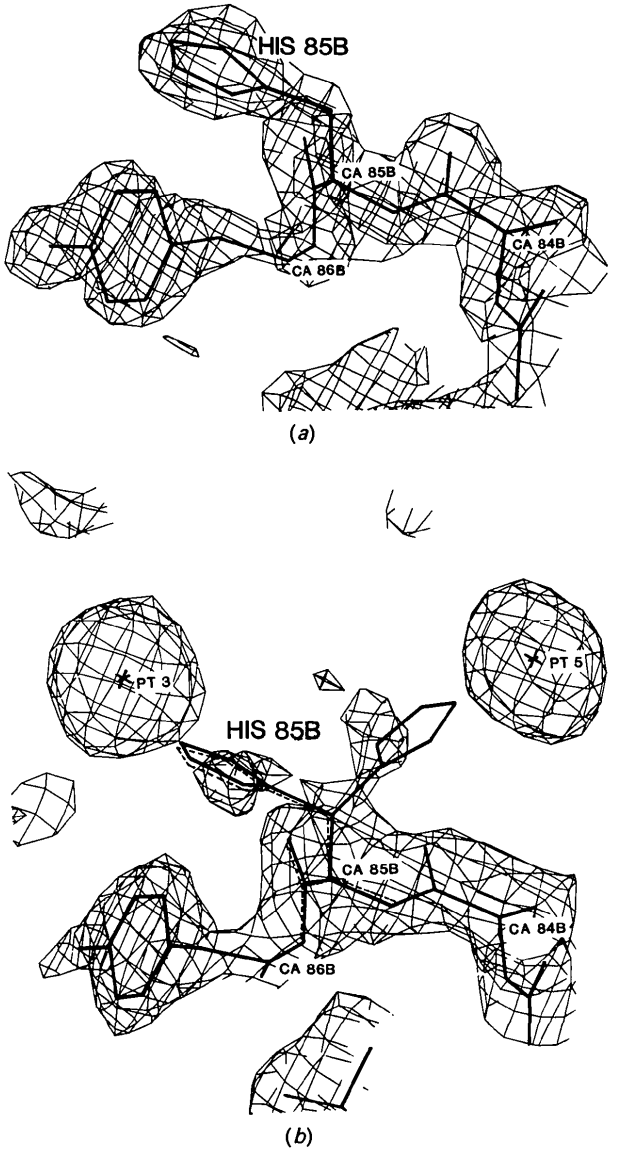

Fig. 3. The electron density for the native (*a*) and the platinum derivative (*b*) at histidine 85 in molecule *B* calculated from the $2F_o - F_c$ and $2F_o(\text{Pt}) - F_c$ Fourier maps respectively and contoured at the same level. The dotted lines in (*b*) correspond to the histidine 85 conformation assumed in the native enzyme. The disorder in the Pt position at histidine 85 is clear but the electron density of the imidazole rings is not well defined.

All of the amino-acid residues were identified in electron density maps, and were in agreement with the primary structure. At the site of the Arg 63 residue in molecule *A*, which is remote from the active site, a nicely shaped tetrahedron-like peak of strong electron density was observed to which the atomic positions of an SO_4^{2-} anion were assigned. The position of this anion is fixed relative to the enzyme by six hydrogen bonds. Two of the bonds are to the amide groups of the Arg 63 and Thr 64 residues, two with Arg 63 NE and NH2 atom and two with Arg 68 NH1 and NH2 atoms of the neighbouring *B* molecule. This electron density was not distinct in molecule *B* owing to the different intermolecular contacts which generate different conformations of the Arg 63 side chain. Instead of the anion a water molecule was found to be localized there.

Water molecules were easily identified as spherical peaks of electron density, often well resolved from their protein and water neighbours, and making chemically and sterically sensible H-bond contacts. Some 239 water molecules were located in the asymmetric unit. They were treated as O atoms in which the position and thermal parameters were refined and the occupancy held at unity. This was an approximation since the dynamic character of the water structure may well lead to incomplete occupancy at some sites. However, the generally reasonable value of the thermal parameters made this an acceptable approximation. There was a tendency for some water molecules to move outside the electron density peak centres during refinement; this was more pronounced when the *B* factor was high. Displaced water molecules were repositioned back to the centres at the end of refinement and then subjected to several more cycles of *B*-factor refinement. Fig. 6 illustrates a group of water molecules which lie between the *A* and *B* molecules in the crystal.

The average *B* value for protein atoms is 17·6 $Å^2$ in molecule *A* and 19·2 $Å^2$ in molecule *B* ($5 < B < 65$ $Å^2$); for water molecules it is 35·7 $Å^2$ ($14 < B < 58$ $Å^2$), while for the sulfate anion atoms it is 22·5 $Å^2$. Out of a total of 239 water molecules, 46 have temperature factors greater than 50 $Å^2$. These were checked in the electron density map and as they satisfied all other criteria for a water molecule they were not deleted from the coordinate file. Thermal parameters of this magnitude are physically reason-

able as water molecules are often only weakly held by H-bonding contacts and are able to vibrate considerably. It is also possible that these sites are not fully occupied, which will lead to apparently higher thermal parameters.

The enzyme–3′-GMP complex: crystal structure (2)

In the refinement of the isomorphous RNase Sa–3′-GMP complex structure, 17 105 reflections in the range 10–1·8 Å were employed. The atomic positions of the native enzyme at $R = 0{\cdot}225$ were used as the initial set of coordinates. The starting R value for the enzyme complex was 0·29. The structure was refined very easily in 80 cycles alternating eight times with rebuilding. The refinement converged with $R = 0{\cdot}175$; the progress in these calculations is illustrated in Fig. 5(*b*).

An attempt was made to refine the enzyme complex using only the principal data set for which $R_{\rm merge} = 0{\cdot}052$, excluding the blind region which merged poorly ($R_{\rm merge} = 0{\cdot}117$) with the principal data. The crystallographic R factor was approximately 1% higher than that obtained with the complete set of data.

Disorder in the side-chain conformation was observed for a number of side chains; that of Cys 72*B* (SG) is illustrated in Fig. 7. This phenomenon was taken into account in the refinement where at these side chains alternative atomic positions were included in the coordinate file with occupancies of 0·6 (0·4) for Cys 72*A* and 0·7 (and 0·3) for Cys 72*B* (estimated from electron density distribution).

Very clear electron density for 3′-GMP was found at the active site of molecule *A* and is shown in Fig. 8. The determination of all 24 3′-GMP atoms was unambiguous. These atoms were included in the refinement only in the final stages. The average temperature-factor value, B, was 26·75 Å^2 ($19 < B < 35$ Å^2). 3′-GMP is not bound to the second molecule. The reason for this became clear after placing 3′-GMP in the *B* molecule active site corresponding to its position in molecule *A*: a hydrogen bond formed by the Arg 65*B* NH2 group with the Asn 20*A* OD1 atoms from a neighbouring molecule prevents binding of the 3′-GMP phosphate group to the catalytic site.

A well-defined sulfate anion was clearly identified at the site of the Arg 63 residue in molecule *A* in the same conformation as that in the native enzyme and with an average temperature factor, B, of 22·3 Å^2. Similar electron density was found at the equivalent site in molecule *B*. Here, however, the temperature factors for the sulfate-ion atoms are significantly

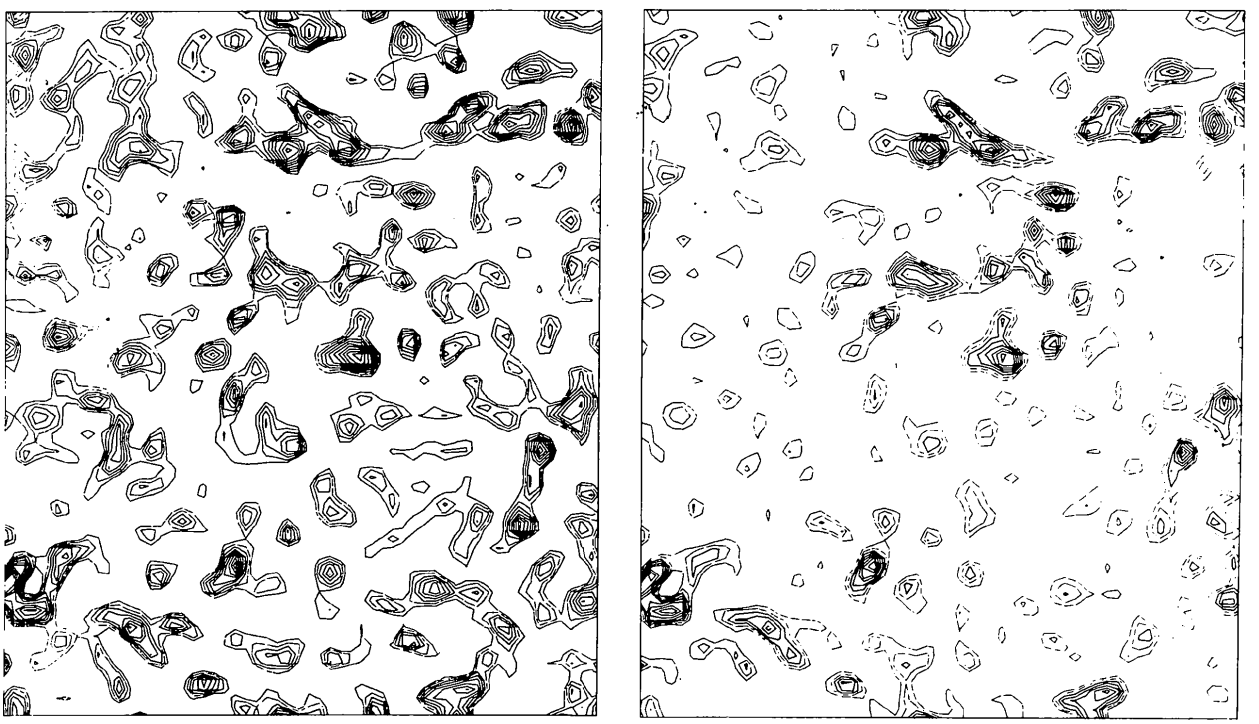

(*a*) (*b*)

Fig. 4. (*a*) An electron density section 8 ($z = 8/120$) calculated at 2·5 Å resolution for the isomorphously phased map and (*b*) the same section after solvent flattening; the electron density of the protein atoms is enhanced and false connections are often lost.

larger, the average B value being 59·8 Å^2. This higher value is a result of there being more space for movement and the existence of only two hydrogen bonds formed with the amide groups of the Arg 63 and Thr 64 residues.

The average value of the thermal parameters for the protein atoms in molecule A is 16·8 Å^2, and in molecule B it is 19·4 Å^2 ($4 < B < 59$ Å^2). In the asymmetric unit, 223 water molecules were found with an average temperature factor of 33·1 Å^2 ($11 < B < 56$ Å^2). In this structure the B factor exceeds 50 Å^2 for only eight water molecules in spite of the fact

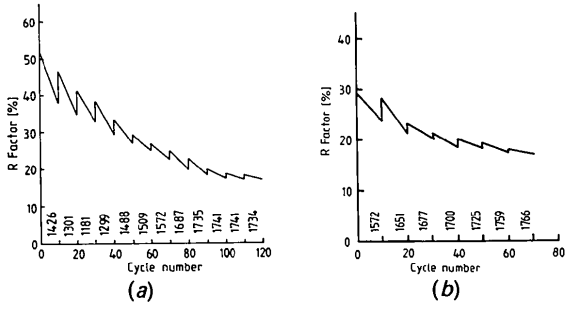

Fig. 5. (*a*) The R value in the course of refinement of the native enzyme [crystal structure (1)]. The starting R value is 0·52, the final R is 0·172. Numbers of atoms included in individual steps of refinement are given at the bottom. In the refinement 17 579 reflections were used in the range 10–1·8 Å. (*b*) The R value in the course of refinement of the enzyme–3′-GMP complex [crystal structure (2)]. The final R value is 0·175. In the refinement 17 105 reflections were used in the range 10–1·8 Å.

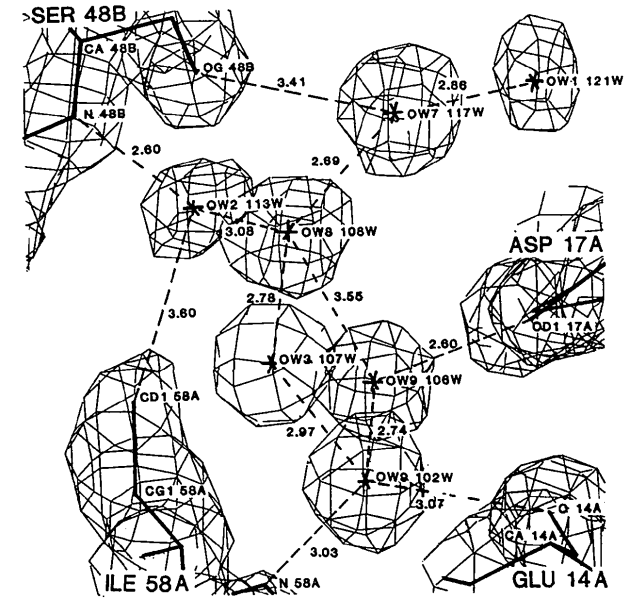

Fig. 6. A group of water molecules which lie between the A and B molecules and which link the protein surfaces through an H-bonded network. Distances are given in Å.

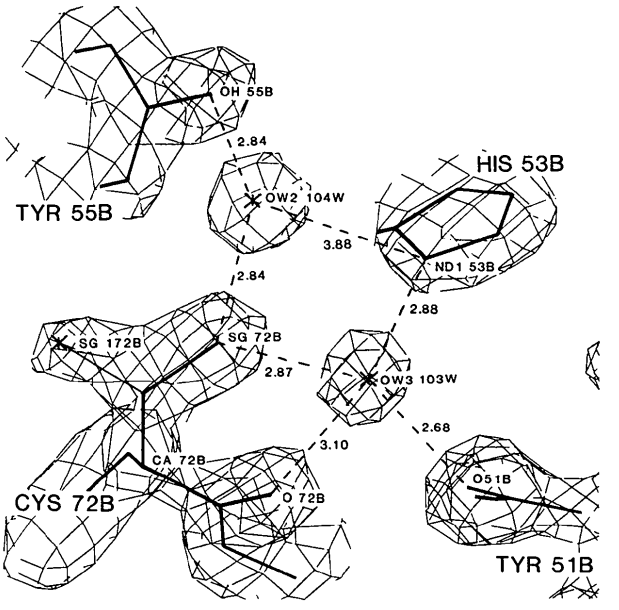

Fig. 7. The electron density at Cys 72 molecule B calculated as the $2F_o - F_c$ map. There are evidently two positions for the SG. Distances are given in Å.

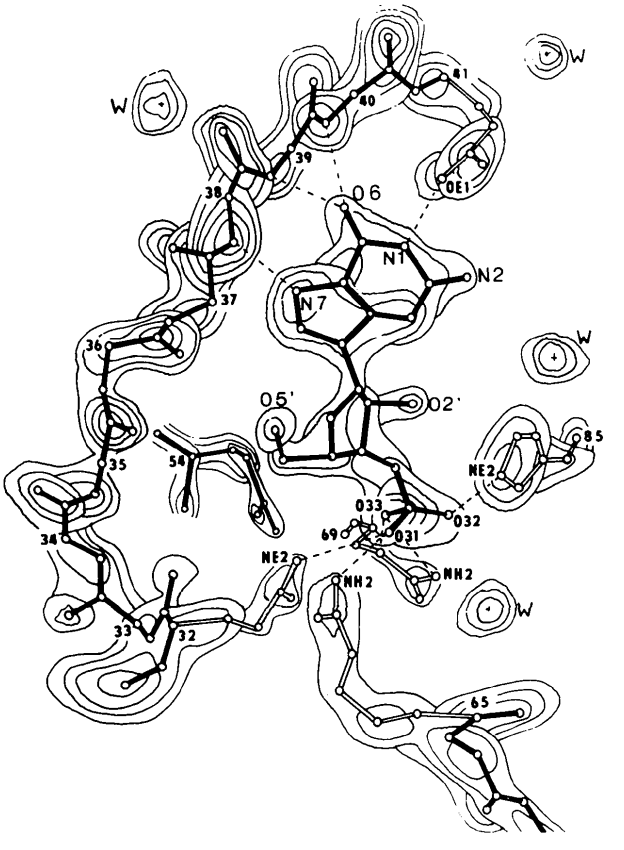

Fig. 8. The electron density of the 3′-GMP and surrounding protein structure. Contour levels are between 0·5 and 2·0 e Å^{-3}.

Table 4. *Comparison of refinement parameters of the native enzyme [structure (1)] and the enzyme–3′-GMP complex [structure (2)]*

Restraints	Structure (1), R_{cryst} = 0·172* Number	R.m.s.	σ	Structure (2), R_{cryst} = 0·175* Number	R.m.s.	σ
Distance restraint information						
Bond distance	1532	0·022	0·020	1563	0·023	0·020
Angle distance	2100	0·059	0·040	2146	0·059	0·040
Planar 1–4 distance	554	0·072	0·060	554	0·069	0·060
Overall deviation from planes	266	0·018		267	0·019	
Chiral centre information						
Chiral volumes	234	0·160	0·120	238	0·171	0·120
Non-bonded contacts restraints						
Single-torsion contacts	530	0·190	0·500	529	0·182	0·500
Multiple-torsion contacts	420	0·191	0·500	427	0·221	0·500
Possible H bonds	169	0·187	0·500	144	0·189	0·500
Conformational torsion angles						
Planar 0, 180	200	6·7	20·0	200	5·7	20·0
Staggered (±60, 120)	224	13·7	20·0	224	15·2	20·0
Orthogonal (±90)	26	13·2	20·0	26	13·9	20·0

* $R_{cryst} = \Sigma||F_o| - |F_c||/\Sigma|F_o|$.

that the final refinement procedure was the same as that for the free enzyme.

The final least-squares refinement parameters for both structures are given in Table 4.*

Estimates of error

All 745 non-H atoms were identified in each molecule of both crystal structures. The mean coordinate error was estimated using the method of Luzzati (1952). It gives an estimate of mean coordinate error to be less than 0·20 Å. The least-squares overlap of main-chain atoms of molecules *A* and *B* of both crystal structures, shows that the average displacement is 0·17 and 0·14 Å respectively. The errors in position were estimated further from the extent of the atomic movements when the restraints were removed in a least-squares minimization calculation of the refined coordinates. For both structures after six cycles $R = 0{\cdot}157$ and the r.m.s. differences between the atomic coordinates of the restrained and unrestrained refinement of native enzyme were 0·10 and 0·12 Å for main-chain atoms and for all atoms, respectively.

Description of refined structures

Main-chain structure

The main-chain and secondary structures of the enzyme are illustrated schematically in Figs. 9(*a*) and 9(*b*). The molecule of RNase Sa contains one regular α helix (residues 13–25) and a twisted, three-stranded antiparallel β sheet (residues 51–57, 68–74, 78–82). There are five reverse turns (residues 39–42, 48–51, 59–62, 75–78, 84–87) and just one isolated turn of a 3_{10} helix (residues 7–11). Residues 26–50 connecting the α helix with the first strand of the β-sheet structure form a large loop lying on the surface of the molecule. By contrast, the other loop connecting the two successive β-sheet strands (residues 58–67) projects from the surface of the molecule. The C-terminal residue, Cys 96 and Cys 7 form an S—S bridge. The amino group of the N-terminal residue, Asp 1, makes a hydrogen-bond contact to the Val 43 main-chain O atom in molecules where Asp 1 is not disordered. One of the six proline residues, Pro 27, adopts a *cis* conformation. In the RNase Sa sequence there is an insertion at 76, which is unique to the microbial riobonucleases. This residue, a threonine, is inserted into a surface loop between two of the antiparallel β-sheet strands (see Fig. 9*a*). Here the main chain and side chain make no H-bonding contacts with other protein atoms.

The main-chain structures of the two independent molecules *A* and *B* are overlapped in Fig. 10(*a*). There are a few changes in the main-chain atomic positions caused by crystal contacts. The most pronounced are at residues 60–63, part of the projecting loop 58–67 and the C terminus (see also Fig. 11). Comparison between the main-chain atoms of the unliganded enzyme and liganded enzyme (molecules *A*) is shown in Fig. 10(*b*). The movements are small and exist between residues 30–33 and 85–86 (see also Fig. 11). In Fig. 13(*a*) the enzyme–3′-GMP complex is shown, its main-chain structure represented as Cα atoms, but with the side chains involved in catalysis and specificity drawn in around the bond nucleotide. Fig. 13(*b*) shows the complex with all atoms drawn.

* Atomic coordinates and structure factors of ribonuclease Sa (Reference: 1SAR, R1SARSF) and its complex with 3′-GMP (Reference: 2SAR, R2SARSF) have been deposited with the Protein Data Bank, Brookhaven National Laboratory, and are available in machine-readable form from the Protein Data Bank at Brookhaven. The data have also been deposited with the British Library Document Supply Centre as Supplementary Publication No. SUP 37038 (as microfiche). Copies may be obtained through The Technical Editor, International Union of Crystallography, 5 Abbey Square, Chester CH1 2HU, England.

Side-chain structure

The side chains are generally well-defined; those buried have a *B* factor averaging 12 Å^2 while those on the surface have a value of about 30 Å^2. However, there are exceptions: some residues at the surface have *B* factors as low as 10 Å^2, and some are much higher. Usually the polar surface side chains are hydrogen bonded to solvent ions or other side chains. Disordered structure was observed for residues Asp 1*A*, Asp 25*B*, Gln 32*A*, Gln 38*B*, Arg 40*B*, Glu 41*B* and Gln 77*B* in the free enzyme, and for Asp 1*A*, Asp 25*A*, Gln 32*A*, Arg 40*B*, Glu 41*B* and Cys 72*A* and 72*B* in the 3′-GMP complex. The electron density for most of these residues is not clear and usually lacks connectivity; this is not the case however for Cys 72, as Fig. 7 illustrates. Table 5 lists average side-chain *B* values for residues that are disordered in one or more of the four molecules in the two crystals. The *B* value for a disordered residue is underlined and is generally larger than that of ordered side chains. The exception is Cys 72 where the two discrete conformations are unusually well defined.

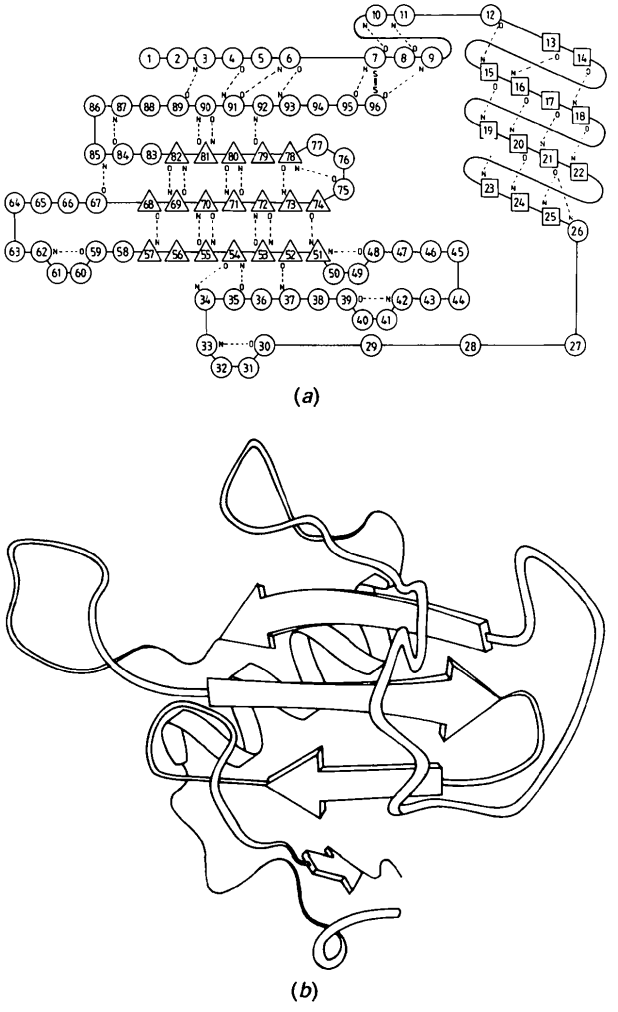

Fig. 9. (*a*) The secondary structure and hydrogen-bonding network in the enzyme. Residues forming the β-sheet structure are shown as triangles, those in the α helix as squares. (*b*) A schematic illustration of the main-chain and secondary structure in the enzyme. Sheets are represented as arrows and the helix (behind the β sheet) by a twisted thread.

Differences in structures

Differences between molecules *A* and *B* of the free and liganded enzyme structures are illustrated graphically in Fig. 11. It can be seen that the differences are most frequent between molecules *A* and *B* in the same crystal (Figs. 11*a* and 11*b*). There are some distinct differences between the free and the liganded enzyme (Fig. 11*c*) and only very few differences between the molecules which are unliganded in both crystal forms (Fig. 11*d*).

The differences in conformation observed between the two crystallographically independent molecules *A* and *B* in the unliganded crystal can mostly be directly attributed to differing crystal contacts (Gln 32, Arg 40, Arg 63, Glu 74, Thr 76, Leu 91). There are some variations in conformation that are a consequence of changes in solvation and side-chain structure some distance from the residues in direct crystal contact (Ser 48, Glu 54 – also affected by alterations in solvent structure following 3′-GMP bonding). The packing of the molecules in the crystal is illustrated in Fig. 12.

It is interesting to note that a significant number of residues making crystal contacts in one molecule have a conformation very similar to their equivalent in the other molecule: (*A*) Cys 7 (N), Asn 20 (OD1), Gln 38 (NE2), Gly 73 (O), Gln 77 (N, OE1), Glu 78 (O), Asp 79 (OD2), Gln 94 (O); (*B*) Glu 14 (OG1, OG2), Pro 29 (O), Tyr 30 (OH), Ser 31 (N, OG), Thr 95 (O). A large proportion of these contacts are made through the main chain which can of course leave the side chain unaffected, particularly if it is well defined by H bonding and other interactions. But in six cases side-chain atoms are involved and in these cases the crystal contacts are clearly made through the already existing conformations.

The arrival of the 3′-GMP in molecule *A*2 has necessarily altered the conformations of several of the residues interacting directly and indirectly with the nucleotide. Thus, Ser 31, Gln 32, Glu 54, Arg 65 and His 85 all move to varying degrees in response to direct contacts to the 3′-GMP molecule. The residues Gln 38, Asn 39 and Arg 40, which interact through the main chain and Glu 41 which interacts through its side chain appear to be a preferred recognition surface for the guanosine base. The changes in confor-

mation at Ser 42 are a consequence of indirect effects involving water-structure changes following the 3′-GMP binding.

The comparison between the two unliganded molecules *B*1 and *B*2 (Fig. 9*d*) shows only one significant difference at residues Arg 40 and Glu 41. In molecule *B* these residues have very high thermal parameters of 55 and 57 Å^2 respectively. Their coordinates are therefore inevitably inaccurate and probably the side chains have more than one conformation. Thus the difference here probably originates from ill-defined atomic positions, not a difference in conformation.

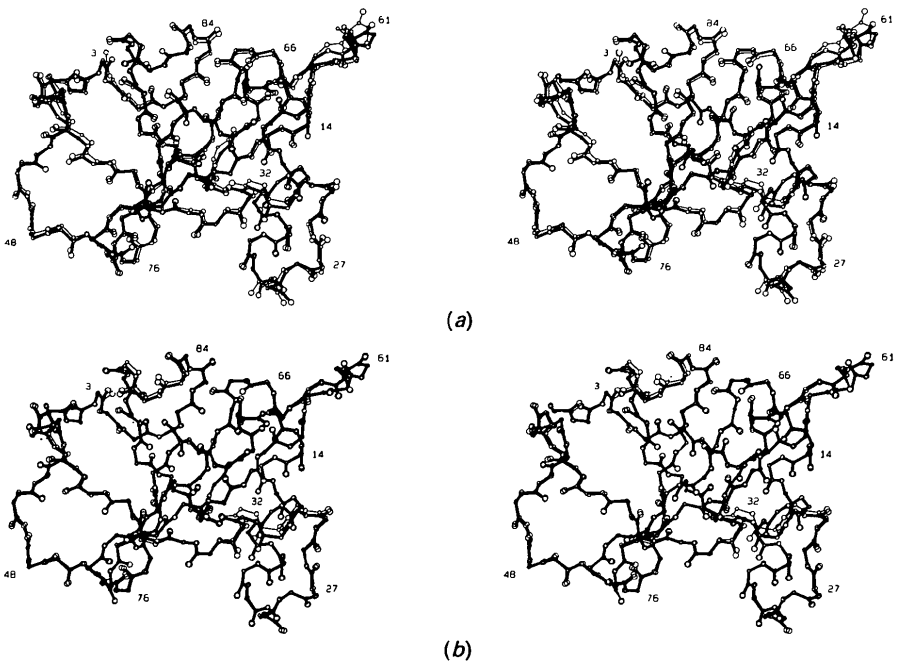

Fig. 10. (*a*) The main-chain atoms of the two independent molecules in the unit cell of structure (1) shown overlapped. The only significant differences occur at residues involved in crystal contacts. (*b*) The main-chain atoms of the free and complexed enzyme (molecule *A*) shown overlapped. The only significant movements at 30–32 and near 85 are a result of 3′-GMP binding.

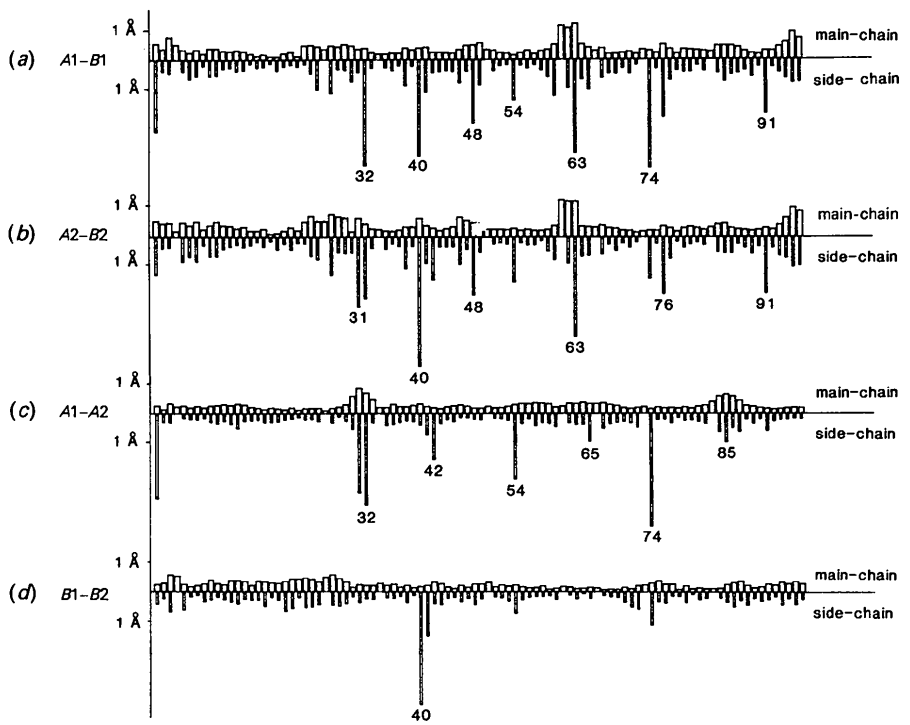

Fig. 11. The r.m.s. deviation represented as histograms of main-chain and side-chain atoms of each residue between molecules overlapped on all atoms by least-squares minimization for (*a*) the native enzyme [crystal structure (1)], molecule *A* overlapped on molecule *B*; (*b*) the 3′-GMP complexed enzyme [crystal structure (2)], molecule *A* (complexed) overlapped on molecule *B* (unbound); (*c*) the native enzyme molecule *A*, overlapped with the 3′-GMP complexed enzyme molecule *A* [crystal structure (2)]; and (*d*) the native enzyme molecule *B* [crystal structure (1)], overlapped with molecule *B* [crystal structure (2)].

Table 5. *Side-chain temperature factors* (Å^2) *of disordered amino-acid residues*

	Mol. *A*1	Mol. *B*1	Mol. *A*2	Mol. *B*2
Asp 1	60·85	36·32	58·38	24·10
Asp 25	48·16	55·22	45·30	36·26
Gln 32	45·88	23·52	46·79	25·45
Gln 38	24·00	42·49	22·30	40·29
Arg 40	36·60	55·06	33·13	61·97
Glu 41	29·08	57·08	19·56	52·42
Cys 72	23·02	27·06	16·34	18·00
Gln 77	30·51	55·35	27·71	40·65

3′-GMP–enzyme (*complex*) structure

As illustrated in Figs. 13(*a*) and 13(*b*), the base of 3′-GMP lies flat on the surface of the molecule in a shallow depression that constitutes the binding site. There are four hydrogen bonds formed between the 3′-GMP base and the enzyme, which can be seen clearly in Fig. 14. Three bonds are with the main-chain groups N38, N39, N40, the fourth with the

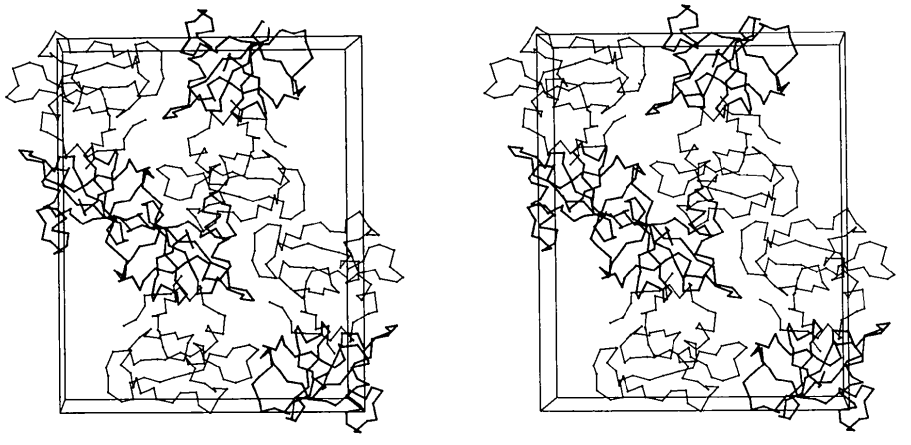

Fig. 12. The packing of the Sa molecules in the crystal shown in stereo. Molecule *A* is drawn as thick lines and molecule *B* as thin lines. Only the main chain, drawn as linked Cα atoms, is shown.

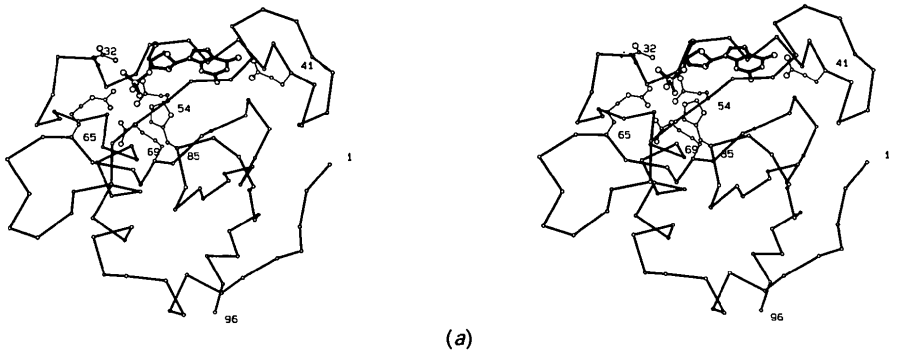

(*a*)

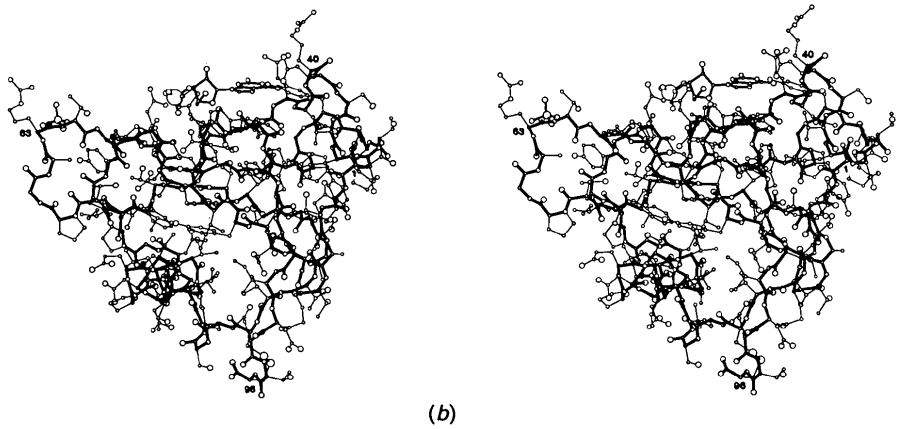

(*b*)

Fig. 13. The substrate-binding pocket and enzyme main-chain structure. (*a*) The enzyme–3′-GMP complex. The 3′-GMP is drawn with thick bonds; the side chains involved in catalysis and binding are shown. The main-chain Cα atoms only are shown. (*b*) The enzyme–3′-GMP complex viewed edge on to the guanine base with all atoms shown. This illustrates the binding site as a relatively shallow cavity.

Glu 41 OE1 atom. The phosphate group makes several hydrogen bonds and salt bridges with Gln 32 (NE2), Arg 65 (NH2), Arg 69 (NE, NH1) and His 85 (NE2). All the bonds are shown in Fig. 8 and listed in Table 6.

The interactions made by the guanosine base with the peptide main chain between residues 38 to 40, illustrated in Fig. 14, explain the critical structural role of Asn 39. There are specific H bonds from both OD1 and ND2 of the Asn 39 side chain to the amide nitrogen 44 and carbonyl oxygen 44 respectively. These contacts help define and stabilize the conformation of the peptide chain between residues 38 and 44 which presents the peptide nitrogens and the glutamic acid 41 to the base in a stereospecific series of contacts. This conformation is essentially identical in all the microbial ribonucleases so far studied; in particular the Asn 39 residue which is crucial to this structure is invariant in all known microbial ribonuclease sequences. The essential character of the Asn 39 residue interactions illustrated in Fig. 14 is demonstrated by Ikehara *et al.* (1986). Their substitution of the Asn 39 residue by aspartic acid in the T_1 enzyme almost completely abolished the enzyme's activity.

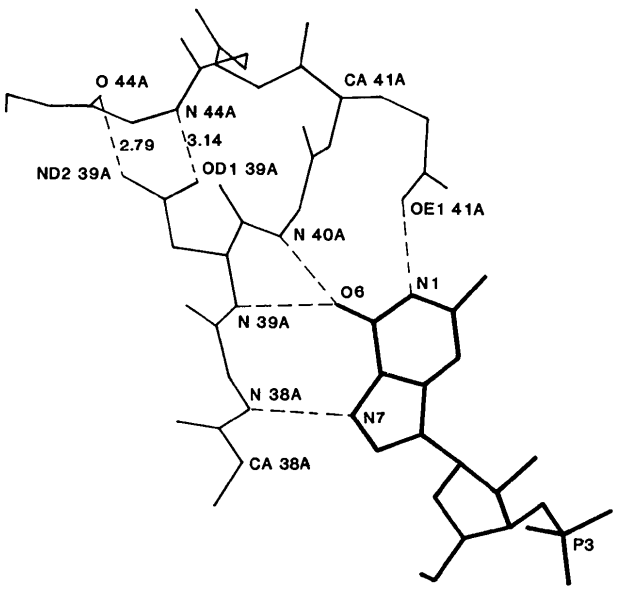

Fig. 14. The hydrogen-bonding contacts (Å) between the guanine and the enzyme and between the Asn 39 side chain and the peptide at 44. These latter interactions contribute to the structure and stability of the specificity pocket.

Table 6. *Contact distances between 3′-GMP and the enzyme*

3′-GMP	RNAse Sa	Distance (Å)	3′-GMP	RNase Sa	Distance (Å)
N7	N 38	2·88	O31	NH2 65	2·78
O6	N 39	2·83	O32	NE2 85	2·54
O6	N 40	2·66	O33	NE 69	3·05
N1	OE1 41	2·63	O33	NH1 69	3·11
O31	NE2 32	3·15	O33	NH2 65	2·80

The catalytic groups at the active site

There are several conformational changes in the enzyme complexed to 3′-GMP (molecule *A*2) evidently caused by binding and already identified in Fig. 11 and illustrated in detail in Fig. 15. The position of the His 85 residue allows it to hydrogen bond to the phosphate oxygen atom upon arrival of the 3′-GMP molecule without moving very much. An inspection of the electron density indicates that the change in its position does not represent a discrete shift of this residue upon ligand binding, but is more a selection of just one of a number of possible conformations present in the free enzyme where it is seen to be partly disordered. The Glu 54 residue is well defined in both structures but its side chain is required to move in the complex to avoid a clash with the 3′-GMP C5′ atom, with which it makes a short contact, 2·79 Å through its OE2 atom. Large apparent changes in the side chain were observed for the Ser 31 residue. The adjacent residue, Gln 32, is involved in the phosphate-group binding. This interaction might have introduced a change in the position of the main-chain atoms facilitating rotation of the Ser 31 side chain around the Cα—Cβ bond and the creation of a hydrogen bond to the neighbouring molecule's main chain. This intermolecular hydrogen bond is made possible not only by reorientation of

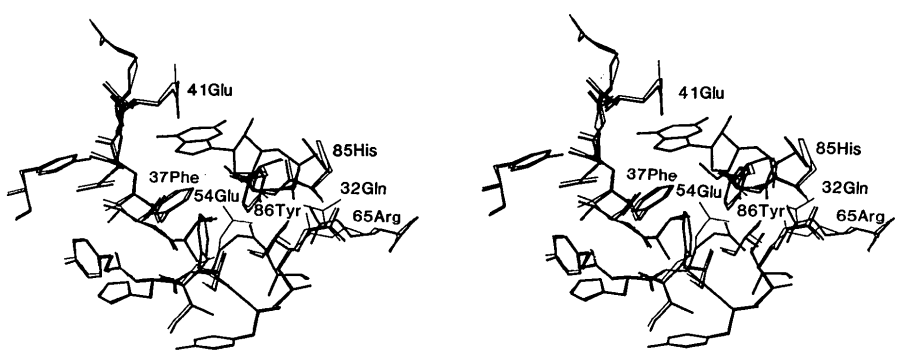

Fig. 15. A stereoview of the 3′-GMP substrate from its binding site (thick lines). The binding residues in the unliganded enzyme (thin lines) are also overlapped. The major movements are seen at residue Glu 54.

the Ser 31 side chain, but also by a shift in main-chain atom positions of up to 1·2 Å and *vice versa*. There are also small movements of the Arg 65 side-chain guanadinium group which forms a hydrogen bond with the phosphate oxygen atom and that of the Glu 41 residue which by its OE1 atom binds the 3′-GMP base.

In the crystal complex the 3′-GMP ribose moiety adopts C(2′)-*endo* type puckering and the torsion angle around the glycosyl link is in the *anti* range. The most widely accepted catalytic mechanism involves proton abstraction from the 2′-hydroxyl by the Glu 54 residue. In the crystal structure, however, this hydroxyl is 7·0 Å from the Glu 54 carboxylate and is 4·6 Å from the nearest protein atom. Thus, the observed nucleotide conformation is not expected to be associated with catalysis since the O2′ atom is directed away from the 54 glutamic acid carboxylate group. The observed conformation is, however, the only one allowed for the 3′-GMP ribose ring in the crystal owing to the intermolecular contacts in the lattice. Surprisingly the same conformation of the ribose ring with respect to the base and phosphate group was found in the RNase Bi–3′-GMP complex where there are no steric hindrances (Sanishvili, 1988). This suggests that the conformation seen is intrinsic for the product of reaction catalysed by these enzymes.

The somewhat different T_1 ribonuclease mechanism of action in which the His 40 and His 92 residues, but not the Glu 58 residue are indispensable for the catalytic activity of the enzyme (Nishikawa *et al.*, 1987) cannot be relevant to RNase Sa as, first, the residue equivalent to T_1 His 40 in Sa is valine, which has no chemical similarity whatsoever, and secondly, there is in Sa no His residue spatially near the Glu 54 residue (RNase T_1 Glu 58 and His 92 correspond to RNase Sa Glu 54 and His 85, respectively).

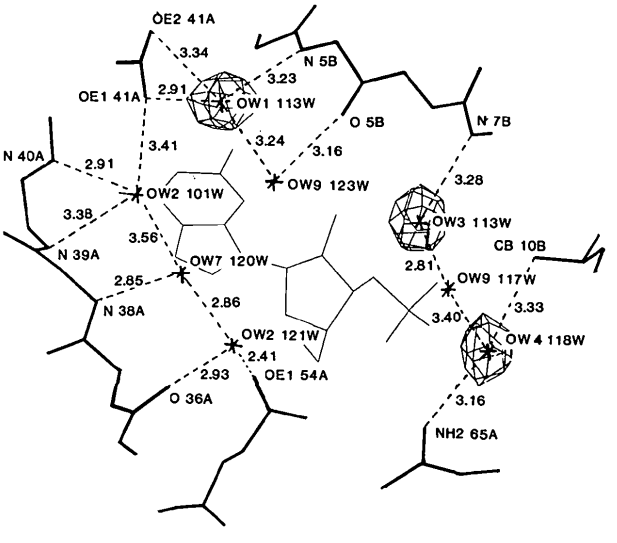

Fig. 16. The water structure in the nucleotide binding site. Asterisks represent water molecules displaced by 3′-GMP; the electron density of those not displaced is shown. Note that O*W*2 101 *W*, O*W*7 120 *W* and O*W*9 117 *W* correspond to atoms in the nucleotide which are hydrogen bonded to the protein. Distances are given in Å.

Displacement of water by 3′-GMP in the complex

The binding of the 3′-GMP inhibitor displaces five well-defined water molecules, which form a network in the bonding cavity, illustrated in Fig. 16. Three other water molecules previously connected by H bonds to the displaced waters, remain held by H bonds to protein main-chain and side-chain atoms. In three cases the water molecules are replaced by H-bonding atoms in the 3′-GMP. Thus O*W*2 101 *W* is replaced by O6, O*W*7 120*W* by N7 and O*W*9 117*W* by a phosphate oxygen. This means that the 3′-GMP molecule is largely able to compensate for the H-bonding energy of the water and at the same time generates a favourable entropy term by releasing the water molecules into the bulk phase.

Concluding remarks

Precise knowledge of the tertiary structure of RNase Sa and its complex with 3′-GMP as obtained by X-ray diffraction techniques has made it possible to identify the residues responsible for specificity and to recognize at least some of the interactions made by the enzyme during catalysis. It has been shown that the few amino-acid residues invariant among all microbial ribonucleases are in a position to have specific roles in catalysis or specificity. The conformation of the 3′-GMP in the enzyme complex in this crystal does not fit the established mechanism of catalysis or suggest an obvious alternative. This inconsistency may be explained if possible motions of the enzyme and substrate during catalysis are considered; modelling suggests that rotation of the ribose ring to yield an active conformation may occur (C. P. Hill, unpublished work). Crystallographic studies of other complexes such as 5′-GMP and 2′-GMP are underway; it is hoped that these structures will further illuminate details of the catalytic mechanism.

We thank the Royal Society for support and the SERC for a Senior Visiting Fellowship (JS). Dr Chris Hill, Dr Fritjof Korber and Dr Leo Brady are thanked for their contribution to data collection. We also thank Dr Chris Hill for valuable discussions on the enzyme's catalysis and specificity and for his reading of the manuscript. The staff at the SRS (Daresbury Laboratory) are thanked for their assistance in data collection.

References

BACOVA, M., ZELINKOVA, E. & ZELINKA, J. (1971). *Biochim. Biophys. Acta*, **235**, 335–338.
BLOW, D. M. & CRICK, F. H. (1959). *Acta Cryst.* **12**, 794–802.
BOTH, V., ZACHAR, J. & ZELINKA, J. (1983). *Gen. Physiol. Biophys.* **2**, 269–278.
DODSON, E. J. (1975). *Crystallographic Computing Techniques*, edited by F. R. AHMED, pp. 259–268. Copenhagen: Munksgaard.
EVANS, P. R. (1987). *Computational Aspects of Protein Crystal Data Analysis. Proceedings of the Daresbury Study Weekend*, edited by J. R. HELLIWELL, P. R. MACHIN & M. Z. PAPIZ, pp. 58–65. Daresbury, UK: Science and Engineering Research Council.
FINDLAY, D., HERRIES, D. G., MATHIAS, A. P., RANBIN, B. R. & ROSS, C. A. (1961). *Nature (London)*, **190**, 781–784.
GASPERIK, J., PRESCAKOVA, S. & ZELINKA, J. (1982). *Biologia*, **36**, 377–381.
HENDRICKSON, W. A. (1985). *Methods Enzymol.* **115**, 252–270.
HENDRICKSON, W. A. & KONNERT, J. H. (1980). *Computing in Crystallography*, edited by R. DIAMOND, S. RAMASESHAN & K. VENKATESAN, pp. 1310–1323. Bangalore: Indian Academy of Sciences.
HILL, C. P., DODSON, G. G., HEINEMANN, U., SAENGER, W., MITSUI, Y., NAKAMURA, K., BORISOV, S., TISCHENKO, G., POLYAKOV, K. & PAVLOVSKY, S. (1983). *TIBS*, **8**, 364–369.
IKEHARA, M., OHTSUKA, E., TOKUNAGA, T., NISHIKAWA, S., UESIGI, S., TANAKA, T., AOYAMA, Y., KIKYODANI, S., FUKIMOTO, K., YAMASE, K. FUCHIMURA, K. & MORIOKA, H. (1986). *Proc. Natl Acad. Sci. USA*, **83**, 4695–4699.
JONES, T. A. (1978). *J. Appl. Cryst.* **11**, 268–272.
LUZZATI, V. (1952). *Acta Cryst.* **5**, 802–810.
NISHIKAWA, S., MORIOKA, H., KIM, H., FUCHIMURA, K., TANAKA, T., UESUGI, S., HAKOSHIMA, T., TOMITA, K., OHTSUKA, E. & IKEHARA, M. (1987). *Biochemistry*, **26**, 8620–8624.
NORTH, A. C. T., PHILLIPS, D. C. & MATHEWS, F. S. (1968). *Acta Cryst.* A**24**, 351–359.
SANISHVILI, R. G. (1988). Personal communication.
SEVCIK, J., GASPERIK, J. & ZELINKA, J. (1982). *Gen. Physiol. Biophys.* **1**, 255–259.
SHLYAPNIKOV, S. U., BOTH, V., KULIKOV, V. A., DEMENTIEV, A. A., SEVCIK, J. & ZELINKA, J. (1986). *FEBS Lett.* **209**, 335–339.
TAKAHASHI, K. (1970). *J. Biochem. (Tokyo)*, **67**, 833–839.
TAKAHASHI, K. & MOORE, S. (1982). *The Enzymes*, 3rd ed., Vol. 15, *Nucleic Acids*, Part B, pp. 435–467. New York: Academic Press.
VIJAYAN, M. (1980). *Acta Cryst.* A**36**, 215–310.
WANG, B. C. (1985). *Methods Enzymol.* **114**, 90–112.
WILSON, K. S. (1978). *Acta Cryst.* B**34**, 1599–1608.
WINKLER, F. K., SCHUTT, C. E. & HARRISON, S. C. (1979). *Acta Cryst.* A**35**, 901–911.
ZELINKOVA, E., BACOVA, M. & ZELINKA, J. (1971). *Biochim. Biophys. Acta*, **235**, 343–344.

Acta Cryst. (1991). B**47**, 253–266

Electron Distributions in Peptides and Related Molecules. 1. An Experimental and Theoretical Study of *N*-Acetyl-L-tryptophan Methylamide

BY MOHAMED SOUHASSOU, CLAUDE LECOMTE,* ROBERT H. BLESSING† AND ANDRÉ AUBRY

Laboratoire de Minéralogie et Cristallographie, URA CNRS 809, *Université de Nancy* I, *Faculté des Sciences, BP* 239, 54506 *Vandoeuvre les Nancy CEDEX, France*

MARIE-MADELEINE ROHMER, ROLAND WIEST AND MARC BÉNARD

Laboratoire de Chimie Quantique, ER 139 *au CNRS, Université Louis Pasteur*, 4 *rue Blaise Pascal*, 67000 *Strasbourg, France*

AND MICHEL MARRAUD

Laboratoire de Chimie Physique Macromoléculaire, URA CNRS 494, *ENSIC INPL, BP* 451, 54001 *Nancy CEDEX, France*

(*Received* 19 *January* 1990; *accepted* 24 *September* 1990)

Abstract

The thermal vibrations and electron density of *N*-Ac-L-Trp-NHMe have been analyzed using single-crystal X-ray diffraction data measured at 103 K with Mo $K\alpha$ radiation to a resolution corresponding to $(\sin\theta_{max})/\lambda = 1{\cdot}17$ Å^{-1}. Measurements of 10 527 reflections gave 4913 unique data [$R_{int}(|F|^2) = 0{\cdot}019$] of which 2641 had $I > 3\sigma(I)$. A multipolar atomic density model was fitted [$R(|F|) = 0{\cdot}028$] in order to calculate phases for the crystal structure factors and map the valence-electron distribution. The phase problem for determining deformation densities by Fourier synthesis for noncentrosymmetric crystals is discussed. The experimental density agrees well with the theoretical density from an *ab initio* SCF molecular wave function calculated at the

* Author to whom correspondence should be addressed.
† Permanent address: Medical Foundation of Buffalo, 73 High Street, Buffalo, New York 14203, USA.

0108-7681/91/020253-14$03.00